Journal of Molecular Liquids xxx (xxxx) xxx

Contents lists available at ScienceDirect

Journal of Molecular Liquids

journal homepage: www.elsevier.com/locate/molliq

Polymer directed synthesis of NiO nanoflowers to remove pollutant from wastewater

Samira Munkaila [a], John Bentley [a,b], Keith Schimmel [b], Tansir Ahamad [c], Saad M. Alshehri [c], Bishnu Prasad Bastakoti [a,b,*]

[a] Department of Chemistry, North Carolina Agricultural and Technical State University, Greensboro, NC 27411, USA
[b] Applied Science and Technology Program, North Carolina Agricultural and Technical State University, Greensboro, NC 27411, USA
[c] Department of Chemistry, College of Science, Bld#5, King Saud University, Riyadh, Saudi Arabia

ARTICLE INFO

Article history:
Received 8 July 2020
Received in revised form 11 October 2020
Accepted 26 October 2020
Available online xxxx

ABSTRACT

Nickel oxide (NiO) nanoflowers are synthesized via a one-pot method using an amphiphilic block copolymer in aqueous solution. Pluronics F-127 block copolymer works as a structure-directing agent in the formation of the NiO nanoflowers. The controlled hydrolysis of the precipitating agent slowly releases ammonia that can form $Ni(OH)_2$, which is stabilized in the polymer solution. The calcination removes the polymeric part of the nanocomposite and converts $Ni(OH)_2$ into NiO with a face-centered cubic (FCC) phase. The synthesized NiO nanoflowers possess a mesoporous structure with an average surface area of 154 m^2/g. Physisorption and electrostatic interactions between negatively charged congo red (CR) and positively charged NiO nanoflowers allow the adsorption of CR dye at ambient conditions. The adsorption of dyes follows pseudo-second-order kinetics, and the adsorbents are regenerated by calcination and recycled three times at similar efficiencies.

Published by Elsevier B.V.

1. Introduction

Nickel oxide (NiO), a transition metal oxide, is recognized as a low-cost material with excellent chemical and electronic properties. It has been used in applications such as catalysts, electrochemical capacitors, fuel cells, and lithium-ion batteries [1–4]. Recently, efforts have been devoted to synthesizing porous NiO for the treatment of organic pollutants in wastewater [5]. NiO has also gained recognition as a photocatalytic adsorbent and, with the incorporation of other metal oxides, for efficient removal of the organic/inorganic pollutants from wastewater [6–9].

Some pollutants (dyes) are hazardous to humans and can result in carcinogenesis and mutagenesis [10,11]. For example, congo red (CR) is a benzidine-based dye mostly used in the textile industry and a toxic organic pollutant, suspected carcinogen, and mutagen [12]. CR exposure has adverse health effects, such as vomiting, cancer, and irritation of skin and eyes, and environmental effects such as disruption of microbial soil respiration [13–15]. Different morphologies of NiO nanomaterials have been synthesized which include nanotubes, nanorods, nanowires, hexagonal nanoplatelets, and nanoflowers to remove dyes from wastewater [16–20].

Among the structures, the nano/microflower structures with thin nanosheets possess an abundance of sites for surface reactions [21,22]. Ci *et al.* synthesized three-dimensional NiO microflowers from two-dimensional nanosheets, which are derived from one-dimensional nanowires [23]. A laboratory synthesized block copolymer was used as a template and structure-directing agent to fabricate sub-30 nm hollow spheres of NiO [24]. A triblock copolymer with core-shell-corona nanoarchitecture served as a designed template for the fabrication of mesoporous nickel ferrite via the micelles assembly approach. The pore size and shell thickness were tuned by changing the molecular structure of block copolymer [25]. The use of block copolymers allows the shape and porosity of the synthesized materials to be controlled at the nanoscale [26,27]. However, the high cost of polymer templates hinders the large-scale synthesis of materials [24,25,28].

Pluronics are relatively cheaper and water-soluble polymers. The hydrophilic-lipophilic balance (HLB) of pluronics plays a vital role in the self-assembly of polymers, which can be tuned by adding salts and surfactants [29–31]. The micellar size could be successfully enlarged, without phase separation, by using a chemically similar, nonvolatile, secondary pluronics polymer as the swelling agent without any chemical conjugation [32]. The structural diversity of these polymers allows synthesizing a wide range of nanoporous materials with controlled morphology [33]. The pore size and connectivity of pores play a vital role in the adsorption of dyes. Tuning the pore size to match the dye enhances the molecule's selectivity and permeability of porous adsorbent [34,35].

This work reports a one-pot hydrothermal synthesis of NiO nanoflowers using pluronics F-127 polymer as a structure-directing

* Corresponding author.
E-mail address: bpbastakoti@ncat.edu (B.P. Bastakoti).

https://doi.org/10.1016/j.molliq.2020.114676
0167-7322/Published by Elsevier B.V.

agent and urea as a precipitating agent in aqueous solution. The use of this polymer not only controls the size of nanoparticles but also supports the thinning of nanosheets. The thin sheets of NiO assemble to form a flower-like structure. These synthesized NiO nanoflowers are observed under both scanning and transmission electron microscopes to determine the morphological characteristics. The porous NiO nanoflowers show excellent adsorption of organic dyes in aqueous solution. The adsorption kinetics are studied to understand the adsorption process of the nanoflowers. The quick adsorption of CR and its removal by calcination allows the NiO to be reusable. The NiO could be recycled by solid/liquid separation followed by heat treatment, suggesting its potential application in wastewater treatment.

2. Experimental section

2.1. Materials

Nickel nitrate hexahydrate [$Ni(NO_3)_26H_2O$; Alfa Aesar], Pluronics F-127 (BASF), urea (Sigma Aldrich), and congo red (Sigma Aldrich) were used as raw materials without further purification.

2.2. Synthesis

$NiNO_3 \cdot 6H_2O$ (0.7 g), urea (0.3 g), and F-127 (0.3 g) were dissolved in 40 mL of deionized water under magnetic stirring for 1 h at room temperature. Then, the greenish transparent solution was transferred into a Teflon-lined, stainless-steel autoclave and kept at 80 °C for 10 h. Afterward, the green precipitate obtained was washed three times with deionized water and dried at room temperature. Finally, the dried samples were calcined in air at 350 °C for 4 h at a ramping rate of 1 °C/min.

2.3. Adsorption of dyes

NiO (0.01 g) was added into 20 mL of a 40 mg/L CR solution. The solution was agitated at room temperature for 100 min. The concentration of adsorbed dyes was spectrophotometrically measured at different time intervals. The amount of CR adsorbed into a unit weight of NiO, Q_e (mg/g) was calculated by using a mass balance equation [36]:

$$Q_e = \frac{(C_0 - C_e)V}{m} \quad (1)$$

where C_o is the initial dye concentration (mg/L), C_e is the dye concentration at equilibrium (mg/L), V is the volume of dye solution (L), and m is the mass of adsorbent used (g).

2.4. Characterization

The morphology and structural analysis of the nanostructure was studied by using a Zeiss Auriga Scanning Electron Microscope (SEM) and a Zeiss Libra 120 kV electron source Transmission Electron Microscope (TEM). Elemental distribution was analyzed with the Zeiss Auriga SEM with Energy-Dispersive x-ray Spectroscopy (EDS). Hydrodynamic diameter and zeta potential were measured using a Malvern Zen3600 Zetasizer. Fourier Transform Infra-Red (FTIR) spectroscopy data were collected with a Shimadzu FTIR equipped with an MCT detector. Thermogravimetric Differential Scanning Calorimetry (TG-DSC) analysis was carried out using a TA-SDT 650 (Discovery series) setup. N_2 adsorption/desorption was determined by a Quantachrom surface area analyzer. The samples were degassed at 150 °C for 8 h. The surface area and pore size distributions were calculated by N_2 adsorption-desorption isotherm using the Brunauer-Emmett-Teller (BET) and Barrett-Joyner-Halenda (BJH) methods, respectively. The crystalline phases were investigated by powder X-ray Diffraction (XRD) (Shimadzu XRD-7000) analysis. Raman spectra were obtained by a Raman spectrometer (Jobin-Yvon T64000). Photocatalytic studies were monitored using a Shimadzu UV-2501 PC spectrophotometer.

3. Results and discussion

$Ni(OH)_2$ was synthesized using the hydrothermal method. The controlled hydrolysis of urea slowly releases ammonia that can form a complex with Ni^{2+} ions. The amino complex of the metal ions is thought to interact with the polyethylene oxide units of the F-127. In this study, the F-127 polymer provides an amphiphilic environment for controlled crystal growth of $Ni(OH)_2$. Calcination at 350 °C simultaneously removes the polymer and transforms $Ni(OH)_2$ into NiO. The thermogravimetric curve (Fig. S1a) for the $Ni(OH)_2$-polymer nanocomposites shows about 12% mass loss at a temperature below 150 °C, which is attributed to the loss of absorbed water. The second weight loss at 250 °C to 350 °C indicates the removal of the polymer as well as decomposition of $Ni(OH)_2$ into NiO. Compared with a polymer containing polystyrene, the F-127 block copolymer is thermally unstable and can be removed at a lower temperature [28].

The infrared spectrum of NiO nanoflowers is shown in Fig. S1b. The signature peaks of polymer disappeared in NiO nanoflowers. The typical wide -OH band of the hydrogen-bonded water molecule was observed at 3500 cm^{-1}. The samples were not protected from moisture during measurements. Nickel ions were observed as the corresponding υ_3 vibrational peaks at approximately 1400 cm^{-1}. A distinct Ni—O stretching and vibrational bands were confirmed at around 830 cm^{-1} and 670 cm^{-1}, respectively [37,38].

The formation of NiO was confirmed by XRD measurement (Fig. 1a). The sharp diffraction peaks of 003, 006, 101, and 110 confirmed the formation of highly crystalline α-$Ni(OH)_2$ before calcination (Fig. S2). The peaks derived from $Ni(OH)_2$ entirely disappeared, and new peaks of 111, 200, 220, 311, and 222 appeared, which are all consistent with the face-centered cubic (FCC) NiO phase (JCPDS No.47–1049). Raman spectroscopy analysis showed that the NiO nanoflowers have peaks of one-photon transverse optical (TO) and longitudinal optical (LO) and two-photon TO and LO, as shown in Fig. 1b.

The porosity of the NiO nanoflowers was analyzed through N_2 adsorption-desorption isotherms (Fig. S3). The synthesized NiO nanoflowers possess a mesoporous structure with a high surface area of 154 m^2/g. The pore size distribution is relatively broad, indicating that the F-127 polymer may not be the perfect template for mesoporous NiO. The use of F-127 polymer gives rise to several ordered mesoporous nanostructures [39–41]. The sol-gel reaction between inorganic precursors and the polymeric template is controlled by the polymerization of alkoxide precursors. The ordered mesoporous NiO is mainly synthesized using a template-free and hard templating method [42,43]. However, in the present study, F-127 polymer works as a structure-directing agent as well as a masking agent to control the overgrowth of crystal. Block copolymers have been employed as an adjustable mask for the synthesis of nanoparticles, which makes the polymer layer on the nanoparticles transform its crystal growth. They are highly resistant to aggregation but, at the same time, fluidic and adjustable to control the growth of the newly formed crystals [44].

The hydrodynamic diameter of the dispersed solution of NiO was measured under dynamic light scattering. Most particles (75%) have a hydrodynamic diameter of ~210 nm, and 25% have ~850 nm diameters (Fig. S4). The low-resolution SEM image (Fig. 2a) reveals nanoflowers with an average diameter of 200–250 nm. The porous nanosheets of NiO self-assembled to form a flower-like structure. The high-resolution SEM images show that the thickness of the individual petals is about 65–75 nm and is well-assembled to form nanoflowers. The slow release of ammonia from urea avoids rapid crystal growth during precipitation. Additionally, the molecularly dissolved urea helps to stabilize nanoparticles.

In the TEM image (Fig. 3) the porosity of petals is seen by the sharp contrast between edges, and the center of the nanoflowers is associated with the interweaving petal subunits at the center, showing suitable

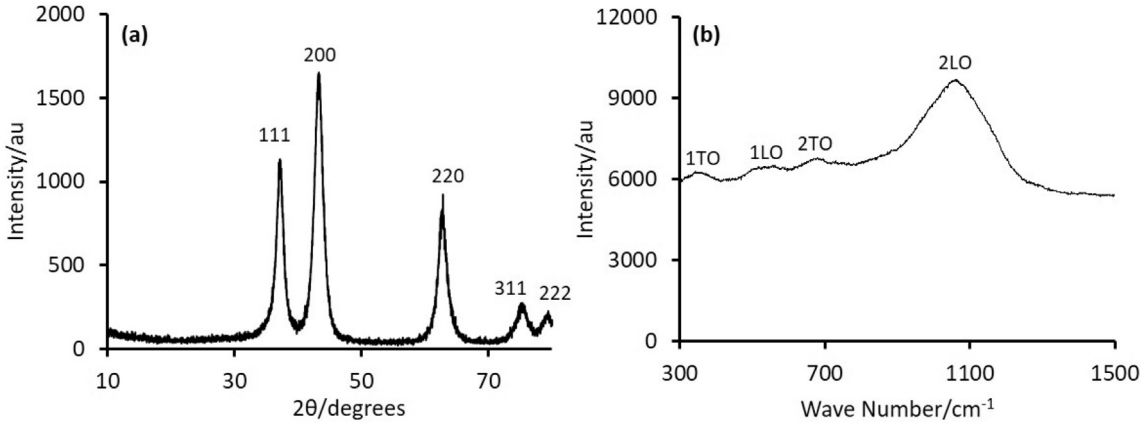

Fig. 1. (a) XRD and (b) Raman spectra of NiO nanoflowers.

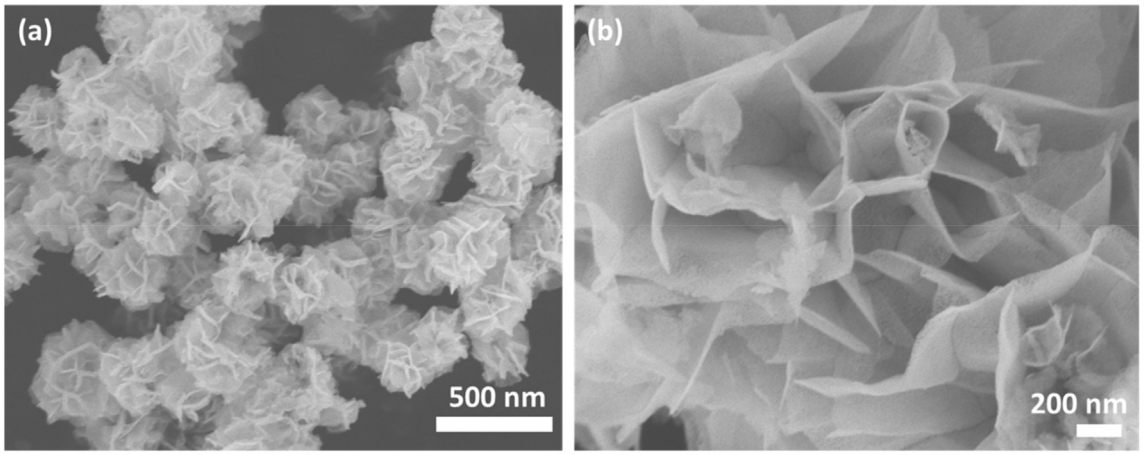

Fig. 2. SEM images of NiO nanoflowers at (a) low and (b) high resolution.

agreement with the SEM observations (Fig. 3). The elemental distribution of NiO nanoflowers was also obtained. It was found that Ni and O were uniformly distributed, as shown in (Fig. S5).

The nanoporous materials have an immense ability to interact with their immediate environment due to their high surface area and pore volume. The adsorbent activity of the NiO nanoflowers was tested

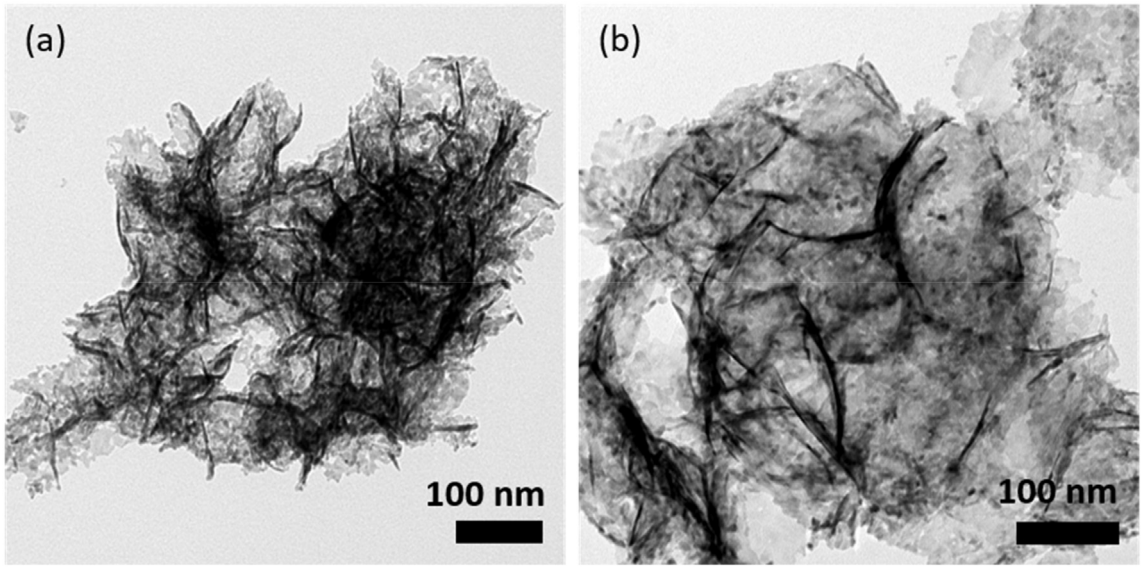

Fig. 3. TEM images of NiO (a) before adsorption and (b) after removing adsorbed CR by calcination for regeneration.

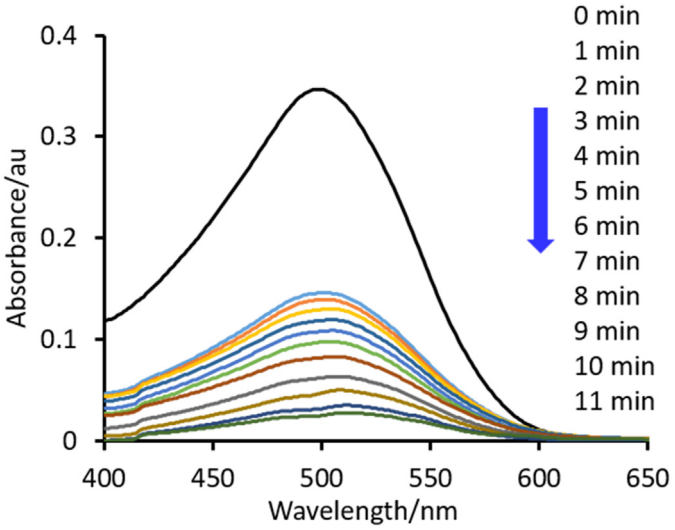

Fig. 4. UV–vis spectra showing the adsorption of the congo red dye by NiO nanoflowers (dye concentration = 5 mg/L, Dose of NiO = 10 mg and volume = 20 mL).

against the CR dye at ambient conditions (Fig. 4). The characteristic absorption peak for CR dye was observed at 497 nm. The adsorption activity of NiO nanoflowers was measured without any equilibration. It was observed that the peak of CR was diminished after 11 min. CR has negatively charged SO_3^- along with organic moieties (Fig. S6). The zeta potential of the synthesized NiO nanoflowers was +28.7 mV. The negatively charged SO_3^- in the CR dye is attracted to the positively charged surface of the NiO nanoflowers through electrostatic interaction [45]. After adsorption of CR onto NiO, the zeta potential decreased to almost zero, indicating that the positive charged NiO is masked by the negatively charged CR dye.

After the first adsorption cycle, the NiO was calcined at 350 °C to remove the previously adsorbed CR dye and to regenerate the adsorbent. After removing the CR dye, the positive surface charges, as well as the morphology of the NiO nanoflowers, were regained. The stability of the adsorbent was examined by TEM observations to establish the effect of adsorption and removal of dyes on the surface morphology and porosity of the material. The TEM images (Fig. 3b) clearly showed the thinning of petals. However, this thinning of petals does not have a significant impact on adsorption capacity as there was a 98% adsorption rate achieved even after the third cycle.

It is interesting to observe the absorption kinetics of the porous NiO nanoflowers [46,47]. To study the adsorption kinetics of CR, pseudo-first-order, pseudo-second-order, and intra-particle diffusion models were evaluated: [48].

Pseudo-first order rate equation:

$$\log(Q_e - Q_t) = \log Q_e - \frac{k_1}{2.303}t \tag{2}$$

Pseudo-second order equation:

$$t/Q_t = 1/k_2 Q_e^2 + t/Q_e \tag{3}$$

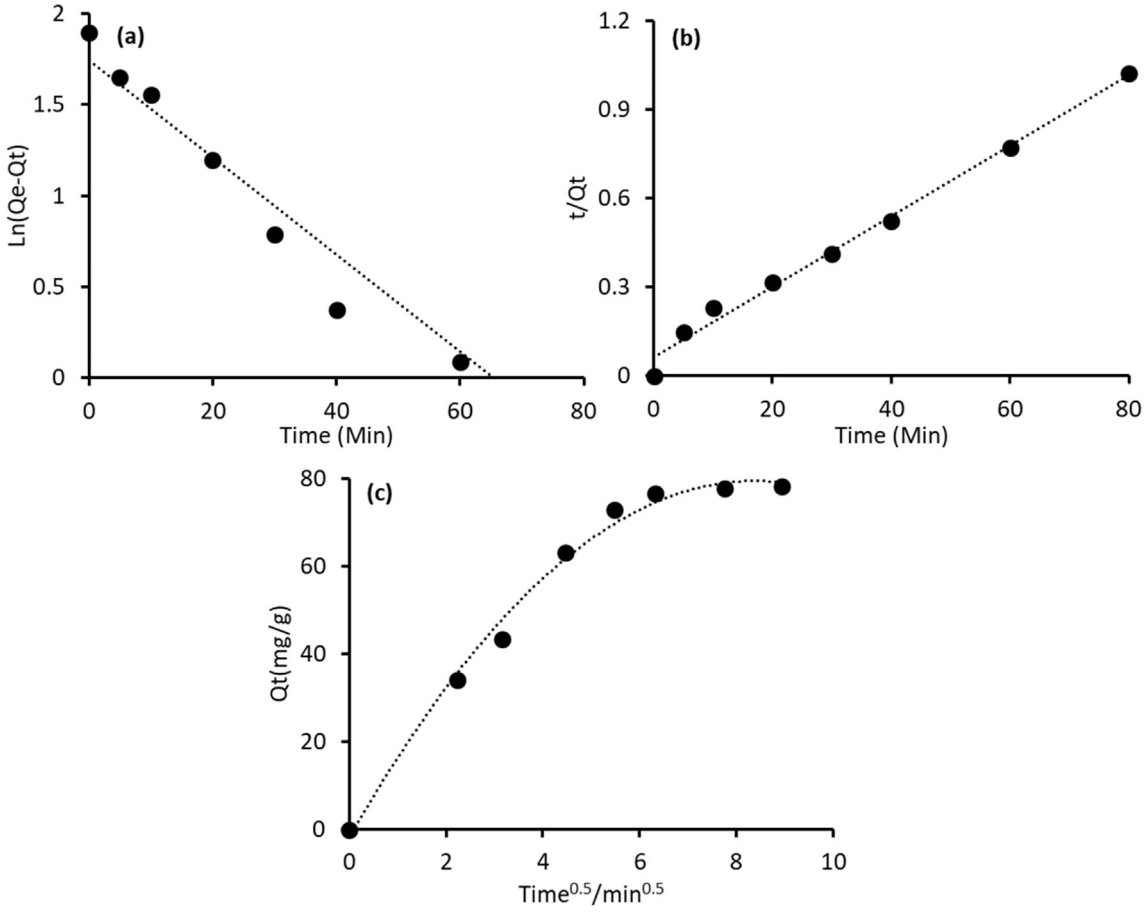

Fig. 5. Kinetic plots of (a) pseudo-first order, (b) pseudo-second order, and (c) intra-particle diffusion model for adsorption of CR onto NiO (dye concentration = 40 mg/L, Dose of NiO = 10 mg and volume = 20 mL).

Intra-particle diffusion model:

$$Q_t = K_3\, t^{0.5} + I \quad (4)$$

where Q_e and Q_t refer to the amount of dye adsorbed at equilibrium and time t, respectively; k_1, k_2, and k_3 are the rate constant for pseudo-first-order, pseudo-second-order, and intra-particle diffusion model; and I is a constant. The validity of the models was verified by the linear equation analysis of $\log(Q_e\text{-}Q_t)$ vs t, t/Q_t vs. t, and Q_t vs $t^{0.5}$, respectively (Fig. 5). The highest correlation coefficient ($R^2 = 0.9905$) was for the pseudo-second-order equation with a rate constant 0.0026 g/mg.min. The kinetics is comparable with other adsorbent used previously [49,50].

4. Conclusion

An amphiphilic block copolymer was successfully used to synthesize porous NiO nanoflowers. Calcination at 350 °C simultaneously removed the polymeric template and converted $Ni(OH)_2$ to NiO. The thin sheet of petals with 65–75 nm thickness assemble to form nanoflowers. The porous nanoflowers possess a high surface area of 154 m^2/g. XRD and Raman spectra showed that the NiO is a face cubic center crystal. The crystalline and porous nanoflowers show a promising result on dye adsorption. The adsorbent activity of the NiO nanoflowers was tested against the anionic CR dye at ambient conditions. The sharp decrease in zeta potential from +28.7 mV to almost zero indicates the strong electrostatic adsorption of CR on NiO. The adsorption kinetics follow the pseudo-second-order model. A reliable and straightforward synthetic method, large adsorption capacity, and fast adsorption rate make the NiO nanoflowers a promising adsorbent for environmental sanitation.

Declaration of Competing Interest

The authors declare that they have no known competing financial interests or personal relationships that could have appeared to influence the work reported in this paper.

Acknowledgments

BPB thanks the National Science Foundation Research Initiation Award (2000310) USA. SMA and TA extend their sincere appreciation to the Deanship of Scientific Research at King Saud University, Saudi Arabia, for funding this Research Group (RG-1435-007). This work was performed in part at the Joint School of Nanoscience and Nanoengineering, a member of the Southeastern Nanotechnology Infrastructure Corridor (SENIC) and National Nanotechnology Coordinated Infrastructure (NNCI), which is supported by the National Science Foundation (Grant ECCS-1542174).

Appendix A. Supplementary data

Supplementary data to this article can be found online at https://doi.org/10.1016/j.molliq.2020.114676.

References

[1] M. Khairy, S.A. El-Safty, M. Ismael, H. Kawarada, Mesoporous NiO nanomagnets as catalysts and separators of chemical agents, Appl. Catal. B Environ. 127 (2012) 1–10.
[2] Y. Jiao, W. Hong, P. Li, L. Wang, G. Chen, Metal-organic framework derived Ni/NiO micro-particles with subtle lattice distortions for high-performance electrocatalyst and supercapacitor, Appl. Catal. B Environ. 244 (2019) 732–739.
[3] D. Xie, Q. Su, W. Yuan, Z. Dong, J. Zhang, G. Du, Synthesis of porous NiO-wrapped graphene nanosheets and their improved lithium storage properties, J. Phys. Chem. C 117 (46) (2013) 24121–24128.
[4] F. Cao, F. Zhang, R. Deng, W. Hu, D. Liu, S. Song, H. Zhang, Surfactant-free preparation of NiO nanoflowers and their lithium storage properties, CrystEngComm 13 (15) (2011) 4903–4908.
[5] L. Ai, Y. Zeng, Hierarchical porous NiO architectures as highly recyclable adsorbents for effective removal of organic dye from aqueous solution, Chem. Eng. J. 215-216 (2013) 269–278.
[6] H. Liu, X. Ren, L. Chen, Synthesis and characterization of magnetic metal–organic framework for the adsorptive removal of Rhodamine B from aqueous solution, J. Ind. Eng. Chem. 34 (2016) 278–285.
[7] J.J. Zhang, F. Cui, L.X. Xu, Q.H. Ma, Y.W. Gao, Y. Liu, T.Y. Cui, Construction of magnetic NiO/C nanosheets derived from coordination polymers for extraordinary adsorption of dyes, J. Colloid Interface Sci. 561 (2020) 542–550.
[8] V. Srivastava, P. Maydannik, M. Sillanpaa, Synthesis and characterization of PPy@NiO nano-particles and their use as adsorbent for the removal of Sr(II) from aqueous solutions, J. Mol. Liq. 223 (2016) 395–406.
[9] B.P. Bastakoti, D. Kuila, C. Salomon, M. Konarova, M. Eguchic, J. Na, Y. Yamauchi, Metal-incorporated mesoporous oxides: synthesis and applications, J. Hazard. Mater. 401 (2021) 123348.
[10] R. Benigni, C. Bossa, Mechanisms of chemical carcinogenicity and mutagenicity: a review with implications for predictive toxicology, Chem. Rev. 111 (4) (2011) 2507–2536.
[11] R.O.A. de Lima, A.P. Bazo, D.M.F. Salvadori, C.M. Rech, D.D. Oliveira, G.D. Umbuzeiro, Mutagenic and carcinogenic potential of a textile azo dye processing plant effluent that impacts a drinking water source, Mutat. Res-Gen. Tox. En. 626 (1–2) (2007) 53–60.
[12] T.M. Reid, K.C. Morton, C.Y. Wang, C.M. King, Mutagenicity of Azo dyes following metabolism by different reductive oxidative systems, Environ. Mutagen. 6 (5) (1984) 705–717.
[13] C. Lu, F. Su, Adsorption of natural organic matter by carbon nanotubes, Sep. Purif. Technol. 58 (1) (2007) 113–121.
[14] L. Sellaoui, M. Kehili, E.C. Lima, P.S. Thue, A. Bonilla-Petriciolet, A.B. Lamine, G.L. Dotto, A. Erto, Adsorption of phenol on microwave-assisted activated carbons: Modelling and interpretation, J. Mol. Liq. 274 (2019) 309–314.
[15] A. Gioxari, D.A.A. Kogiannou, N. Kalogeropoulos, A.C. Kaliora, Phenolic compounds: bioavailability and health effects, in: B. Caballero, P.M. Finglas, F. Toldrá (Eds.), Encyclopedia of Food and Health, Academic Press, Oxford 2016, pp. 339–345.
[16] H.-J. Liu, T.-Y. Peng, D. Zhao, K. Dai, Z.-H. Peng, Fabrication of nickel oxide nanotubules by anionic surfactant-mediated templating method, Mater. Chem. Phys. 87 (1) (2004) 81–86.
[17] W. Wang, Y. Liu, C. Xu, C. Zheng, G. Wang, Synthesis of NiO nanorods by a novel simple precursor thermal decomposition approach, Chem. Phys. Lett. 362 (1) (2002) 119–122.
[18] A. Ali, M. Ammar, A. Mukhtar, T. Ahmed, M. Ali, M. Waqas, M.N. Amin, A. Rasheed, 3D NiO nanowires@NiO nanosheets core-shell structures grown on nickel foam for high performance supercapacitor electrode, J. Electroanal. Chem. 857 (2020) 113710.
[19] S.A. El-Safty, M. Khairy, M. Ismael, H. Kawarada, Multidirectional porous NiO nanoplatelet-like mosaics as catalysts for green chemical transformations, Appl. Catal. B Environ. 123-124 (2012) 162–173.
[20] S. Liu, W. Zeng, T. Chen, Synthesis of hierarchical flower-like NiO and the influence of surfactant, Physica E: Low-Dimen. Syst. Nanostruct. 85 (2017) 13–18.
[21] L. Zhu, W. Zeng, J.D. Yang, Y.Q. Li, Unique hierarchical Ce-doped NiO microflowers with enhanced gas sensing performance, Mater. Lett. 251 (2019) 61–64.
[22] Y. Wang, Q.S. Zhu, H.G. Zhang, Fabrication of beta-$Ni(OH)_2$ and NiO hollow spheres by a facile template-free process, Chem. Commun. 41 (2005) 5231–5233.
[23] S.Q. Ci, Z.H. Wen, Y.Y. Qian, S. Mao, S.M. Cui, J.H. Chen, NiO-microflower formed by nanowire-weaving nanosheets with interconnected Ni-network decoration as supercapacitor electrode, Sci. Rep. 5 (2015) 11919.
[24] M. Sasidharan, N. Gunawardhana, C. Senthil, M. Yoshio, Micelle templated NiO hollow nanospheres as anode materials in lithium ion batteries, J. Mater. Chem. A 2 (20) (2014) 7337–7344.
[25] S. Tanaka, B.P. Bastakoti, S. Yusa, Y. Li, D. Ishii, K. Kani, A. Fatehmulla, W.A. Farooq, M.J.A. Shiddiky, Y. Bando, Y.V. Kaneti, Y. Yamauchi, M.S.A. Hossain, Self-assembly of polymeric micelles made of asymmetric polystyrene-b-polyacrylic acid-b-polyethylene oxide for the synthesis of mesoporous nickel ferrite, Eur. J. Inorg. Chem. 10 (2017) 1328–1332.
[26] B.P. Bastakoti, Y. Li, T. Kimura, Y. Yamauchi, Asymmetric block copolymers for supramolecular templating of inorganic nanospace materials, Small 11 (17) (2015) 1992–2002.
[27] B.P. Bastakoti, S. Guragain, Synthesis of inorganic hollow nanospheres and their application in drug in delivery, J. Nep. Chem. Soc. 38 (2018) 12–17.
[28] B.P. Bastakoti, S. Munkaila, S. Guragain, Micelles template for the synthesis of hollow nickel phosphate nanospheres, Mater. Lett. 251 (2019) 34–36.
[29] L.X. Fan, M. Degen, N. Grupido, S. Bendle, P. Pennartz, Effects of molecular weight, temperature and salt on the self assembly of triblock copolymer solutions, Mater. Sci. Eng. A 528 (1) (2010) 127–136.
[30] S.A. Pillai, U. Sheth, A. Bahadur, V.K. Aswal, P. Bahadur, Salt induced micellar growth in aqueous solutions of a star block copolymer Tetronic (R) 1304: investigating the role in solubilizing, release and cytotoxicity of model drugs, J. Mol. Liq. 224 (2016) 303–310.
[31] A.S. Poyraz, C. Albayrak, O. Dag, The effect of cationic surfactant and some organic/inorganic additives on the morphology of mesostructured silica templated by pluronics, Microporous Mesoporous Mater. 115 (3) (2008) 548–555.
[32] B. Vyas, S.A. Pillai, S. Tiwari, P. Bahadur, Effects of head group and counter-ion variation in cationic surfactants on the microstructures of EO-PO block copolymer micelles, Colloid Interf. Sci. 33 (2019) 100216.
[33] D.R. Dunphy, P.H. Sheth, F.L. Garcia, C.J. Brinker, Enlarged pore size in mesoporous silica films templated by pluronic F127: use of poloxamer mixtures and increased

template/SiO2 ratios in materials synthesized by evaporation-induced self-assembly, Chem. Mater. 27 (1) (2015) 75–84.
[34] X. Yuan, S.P. Zhuo, W. Xing, H.Y. Cui, X.D. Dai, X.M. Liu, Z.F. Yan, Aqueous dye adsorption on ordered mesoporous carbons, J. Colloid Interface Sci. 310 (1) (2007) 83–89.
[35] D.N. Jiang, M. Chen, H. Wang, G.M. Zeng, D.L. Huang, M. Cheng, Y. Liu, W.J. Xue, Z.W. Wang, The application of different typological and structural MOFs-based materials for the dyes adsorption, Coord. Chem. Rev. 380 (2019) 471–483.
[36] N.K. Amin, Removal of direct Blue-106 dye from aqueous solution using new activated carbons developed from pomegranate peel: adsorption equilibrium and kinetics, J. Hazard. Mater. 165 (2009) 52–62.
[37] D.S. Hall, D.J. Lockwood, S. Poirier, C. Bock, B.R. MacDougall, Raman and infrared spectroscopy of α and β phases of thin nickel hydroxide films electrochemically formed on nickel, J. Phys. Chem. A 116 (25) (2012) 6771–6784.
[38] J. Adhikary, P. Chakraborty, B. Das, A. Datta, S.K. Dash, S. Roy, J.W. Chen, T. Chattopadhyay, Preparation and characterization of ferromagnetic nickel oxide nanoparticles from three different precursors: application in drug delivery, RSC Adv. 5 (45) (2015) 35917–35928.
[39] Y. Ren, Z. Ma, P.G. Bruce, Ordered mesoporous metal oxides: synthesis and applications, Chem. Soc. Rev. 41 (14) (2012) 4909–4927.
[40] L.X. Song, Z.K. Yang, Y. Teng, J. Xia, P. Du, Nickel oxide nanoflowers: formation, structure, magnetic property and adsorptive performance towards organic dyes and heavy metal ions, J. Mater. Chem. A 1 (31) (2013) 8731–8736.
[41] L. Kong, J. Zhao, S. Han, T. Zhang, L. He, P. Zhang, S. Dai, Facile synthesis of copper containing ordered mesoporous polymers via aqueous coordination self-assembly for aerobic oxidation of alcohols, Ind. Eng. Chem. Res. 58 (16) (2019) 6438–6445.
[42] M.A. Wahab, F. Darain, Nano-hard template synthesis of pure mesoporous NiO and its application for streptavidin protein immobilization, Nanotechnology 25 (16) (2014) 165701.
[43] L.Q. Lu, P. Andela, J.T.M. De Hosson, Y.T. Pei, Template-free synthesis of nanoporous nickel and alloys as binder free current collectors of Li ion batteries, ACS Appl. Nano Mater. 1 (5) (2018) 2206–2218.
[44] Z.X. Wang, B.W. He, G.F. Xu, G.J. Wang, J.Y. Wang, Y.H. Feng, D.M. Su, B. Chen, H. Li, Z.H. Wu, H. Zhang, L. Shao, H.Y. Chen, Transformable masks for colloidal nanosynthesis, Nat. Commun. 9 (2018) 563.
[45] H.-J. Wang, C.-F. Wang, Y.-Y. Sun, Y. Cao, Film-form dye adsorbents of NiO: synthesis, biological activity and application on dye sorption, Chem. Eng. J. 209 (2012) 442–450.
[46] K.M. Sachin, S.A. Karpe, M. Singh, A. Bhattarai, Self-assembly of sodium dodecylsulfate and dodecyltrimethylammonium bromide mixed surfactants with dyes in aqueous mixtures, R. Soc. Open Sci. 6 (3) (2019) 181979.
[47] K.M. Sachin, S.A. Karpe, M. Singh, A. Bhattarai, Study on surface properties of sodiumdodecyl sulfate and dodecyltrimethylammonium bromide mixed surfactants and their interaction with dyes, Heliyon 5 (2019) e01510.
[48] M. Ayad, N. Salahuddin, A. Fayed, B.P. Bastakoti, N. Suzuki, Y. Yamauchi, Chemical design of a smart chitosan-polypyrrole-magnetite nanocomposite toward efficient water treatment, Phys. Chem. Chem. Phys. 16 (39) (2014) 21812–21819.
[49] V.O. Njoku, K.Y. Foo, M. Asif, B.H. Hameed, Preparation of activated carbons from rambutan (Nephelium lappaceum) peel by microwave-induced KOH activation for acid yellow 17 dye adsorption, Chem. Eng. J. 250 (2014) 198–204.
[50] X.M. Peng, D.P. Huang, T. Odoom-Wubah, D.F. Fu, J.L. Huang, Q.D. Qin, Adsorption of anionic and cationic dyes on ferromagnetic ordered mesoporous carbon from aqueous solution: equilibrium, thermodynamic and kinetics, J. Colloid Interface Sci. 430 (2014) 272–282.